A Hybridized Discontinuous Galerkin Finite Element Method for Multi-Physics Problems

Nicolas Corthouts*
Université de Liège, Aerospace and Mechanics Department, 4000 Liège, Belgium

Koen Hillewaert†
Université de Liège, Aerospace and Mechanics Department, 4000 Liège, Belgium

Georg May‡
von Karman Institute for Fluid Dynamics, 1640 Rhode-Saint-Genèse, Belgium

Thierry Magin§
von Karman Institute for Fluid Dynamics, 1640 Rhode-Saint-Genèse, Belgium

This paper presents one of the first high-order simulations of inductively coupled plasma (ICP). First, a multi-domain solver using a variant of discontinuous Galerkin method, called the hybridized discontinuous Galerkin method, is developed. This multi-domain solver is verified on an analytical conjugate heat transfer problem, showing that the order of convergence is retrieved. Then, the method is extended to the simulation of an inductively coupled plasma, involving the coupled simulation of magnetohydrodynamic flow inside the torch to the Maxwell equations outside. The method is applied to a test case involving the swirled flow of argon and compared to results obtained with finite volume codes. The results are in very good agreement, but further improvements to the coupling boundaries need to be developed to remove small amplitude wiggles at the interface, which have a negative impact on the predicted heat flux.

I. Nomenclature

u	=	Velocity field
T	=	Temperature
$\partial_z p$	=	Pressure gradient
μ_0	=	Void magnetic permeability
η	=	Dynamic viscosity
k	=	Heat conductivity
R	=	Pipe radius in CHT problem
d	=	Pipe thickness in CHT problem
E_I	=	Induced electric field
E_C	=	Coil electric field
E_P	=	Plasma electric field
λ	=	Hybrid unknwon
w	=	State vector
q	=	Gradient of state vector or heat flux
μ, τ, φ	=	Basis functions
^{bc}	=	Quantities relative to a boundary
^{K}	=	Quantities relative to the K^{th} element
^{l}	=	Quantity relative to a domain
C	=	Compatibility condition
F	=	Physical flux
^{c}	=	Quantity relative to convection
^{d}	=	Quantity relative to diffusion
S	=	Source term
Ψ	=	Vector of convected quantities
$m_{1/2}$	=	Averaged momentum
m_p	=	Pressure diffusion low-Mach preconditioner
d	=	Pipe radius in CHT problem
P_J	=	Power dissipated by Joule effect
E_C	=	Coil electric field
σ_e	=	Electric conductivity
f	=	Induction current frequency
τ_{ij}	=	Component of the viscous stress tensor
$\mathcal{T}$	=	Tesselation of the domain
Ω	=	Computational domain
Γ	=	Mesh skeleton
t	=	Time variable

*Ph. D. Candidate, Design of Turbomachines, ncorthouts@uliege.be
†Assistant Professor, Design of Turbomachines, koen.hillewaert@uliege.be
‡Associate Professor, Aeronautics and Aerospace, georg.may@vki.ac.be
§Full Professor, Aeronautics and Aerospace, thierry.magin@vki.ac.be

$\mathcal{N}$	=	Residual of the system	x, r, z	=	Spatial variables
$\mathcal{H}$	=	Numerical flux	n	=	Outward pointing normal
$\mathcal{F}$	=	Interface Condition	$_h$	=	Discretized quantity

II. Introduction

Inductively coupled plasma (ICP) facilities are experimental devices of capital importance in space exploration. By recreating the thermodynamic conditions during atmospheric reentry, they allow for the study of the demise of space debris and thermal shields. The Plasmatron, located at the von Karman Institute for Fluid Dynamics in Belgium, is the most powerful facility of this type in the world. With a power of 1200 kW, it can reach a temperature of 10000 K. The unique features of this facility makes it attractive and led to collaborations with NASA and ESA in the past.

However, ICP are complex facilities, featuring various strongly coupled physical phenomena that need to be correctly predicted to enhance the quality of the tests. Since experimental measurements are not always easy to acquire, the development of numerical methods for capturing the ICP flow correctly are of capital importance. Several codes have been developed in the past, see for instance [1] and [2]. While giving satisfactory results, they were based on the finite volumes method, demanding a high number of elements in the near wall region in order to capture the high temperature gradients arising in the facility. Moreover, low order finite volumes methods are not well suited for studying unsteady features such as instabilities or even turbulence. For this reason, a higher-order accurate discretisation is developed based upon the family of discontinuous Galerkin (DG) methods. In addition, the use of an unstructured discontinuous finite-element like method allows to relax greatly the quality requirements of the mesh, which is very useful for complex geometry and technological features. The present paper displays one of the first simulations of inductively coupled plasmas, using a hybridized discontinuous Galerkin (HDG) method [3, 4].

ICP being a multi-physics problem, one of its main challenges is the multi-domain aspects, in other words the simulation of different strongly coupled physics in separate domains interconnected with specific interface conditions. In this paper, a discretisation technique for these interface connections is developed and applied to two problem types. As a proof of concept, the CHT problem is studied, since an analytical solution can be found. In the CHT, the equations governing the heat transfer in the solid material is a simple heat diffusion equation, while the Navier-Stokes equations are solved in the fluid domain. In the case of inductively coupled plasma (ICP), the full system of Navier-Stokes and electric field equation is solved inside the torch, while only the electric field equation rules the domain outside the facility.

There are two main approaches to multi-domain simulations. The first one is the staggered approach, where the domains are handled separately by stand alone solvers exchanging data. The staggered approach can be either strongly or loosely coupled. The former subiterates until equilibrium is reached, while the latter just performs one forward step successively for each of the domains. The information collected by one domain at its boundary is considered as a known, even though it is the result of the computations from another domain. This approach is conceptually simple and straightforward to implement. However, the method is known to lead to instabilities. There is a large body of literature on stability analysis of coupled method (see for instance *e.g.* [5, 6]). An example of application for inductively coupled plasma can be found in [1, 2].

The second approach is the monolithic one. This time, the system is solved as a whole. This allows for faster and more stable convergence to the solution. However, it is much more complex to implement, and has a strong impact on the system structure as it links the unknowns from one domain to another.

In this work, a fully-coupled approach is developed for the HDG method. To our best knowledge, this strategy has never been tried before in the literature for HDG. The closest examples are found in solution of multi-domain problems with the classic DG method [7]. Consequently, a significant part of this work is dedicated to the development of a HDG multi-domain fully coupled solver.

This work is presented as follows. First, the basis of HDG method and its solution strategy is presented. Next, an extension of the HDG method to multi-domain problems is derived. A comparison of the numerical and analytical solutions of a classic multi-domain case, called the conjugate heat transfer (CHT) problem, is then presented. The specifications of a typical ICP simulation are then given. Finally, an example of a ICP test case is presented.

III. Hybridized discontinuous Galerkin method for single-physics problems

Before discussing our approach to multi-physics HDG, it is useful to describe its single-physics pendant, as they share the exact same mathematical structure. The developments here follow closely [3], [4], [8].

A. Problem statement

Let us consider a domain $\Omega \subset \mathbb{R}^D$ of dimension D with boundary $\partial\Omega$. Let us define the conservative equation over Ω:

$$\begin{aligned} &\partial_t u(x,t) + \nabla \cdot F(u(x,t), \nabla u(x,t)) = S(u(x,t), \nabla u(x,t)), && x \in \Omega, && t \in \mathbb{R}_0^+ \\ &u(x,t) = u_{bc}(x,t), && x \in \partial\Omega_d, && t \in \mathbb{R}_0^+ \\ &\nabla u(x,t) \cdot n = q_{n,bc}(x,t), && x \in \partial\Omega_n, && t \in \mathbb{R}_0^+ \\ &u(x,0) = U(x), && x \in \Omega \end{aligned} \tag{1}$$

where $u : (x,t) \in \Omega \times \mathbb{R}^+ \rightarrow u(x,t) \in \mathbb{R}^N$ is the vector of conserved variables, N is its dimension, $F : (x,t) \in \Omega \times \mathbb{R}^+ \rightarrow F(x,t) \in \mathbb{R}^{N \times D}$ is the physical flux function, and $S : (x,t) \in \Omega \times \mathbb{R}^+ \rightarrow S(x,t) \in \mathbb{R}^N$ represents the source terms. $\partial\Omega_d, \partial\Omega_n \subset \partial\Omega$ are the parts of the boundary where the Dirichlet and Neumann boundary conditions apply respectively. $u_{bc} : (x,t) \in \partial\Omega_d \times \mathbb{R}^+ \rightarrow u_{bc}(x,t) \in \mathbb{R}_D^N$ and $q_{n,bc} : (x,t) \in \partial\Omega_n \times \mathbb{R}^+ \rightarrow q_{n,bc}(x,t) \in \mathbb{R}^{N_N}$ represent the known boundary functions for the state and the nomral component of the gradient state vectors respectively. N_N and N_D represent the number of variables to which a Neumann and a Dirichlet boundary conditions are applied respectively, with $N_D + N_N = N$. Please note that $\partial\Omega_d$ and $\partial\Omega_n$ depend on the variable under consideration. Finally, $U : x \in \Omega \rightarrow U(x) \in \mathbb{R}^N$ represents an initial field.

B. Spatial discretization

If Ω is tessalated in a collection $\mathcal{T}$ of N_e non-overlapping subdomains Ω_K called elements, one has

$$\mathcal{T} = \bigcup_K \Omega_K, \quad \text{and} \quad \Omega_K \bigcap \Omega_{K'} = \emptyset \quad \text{if} \quad \Omega_K \neq \Omega_{K'} \tag{2}$$

Let us also define the set of boundary elements $\partial\mathcal{T}$

$$\partial\mathcal{T} = \{\partial\Omega_K \backslash \partial\Omega : \Omega_K \in \mathcal{T}\} \tag{3}$$

and the mesh skeleton Γ

$$\Gamma = \{e : e = \Omega_K \cap \Omega_{K'} \text{ for } \Omega_K, \Omega_{K'} \in \mathcal{T}, \Omega_K \neq \Omega_{K'}\} \tag{4}$$

We highlight here that each element e of Γ is represented twice in $\partial\mathcal{T}$, and that Γ does not contain $\partial\Omega$.

C. Functional spaces

The purpose of HDG is to find an approximation to the solution u and its gradient $q = \nabla u$ on functional spaces given on Ω and Γ. Let us define the sets of square-integrable functions over Ω and Γ as

$$\begin{aligned} V &= \left\{v : x \in \Omega \rightarrow v(x) \in \mathbb{R}^D, v \in L^2(\Omega)\right\} \\ W &= \left\{w : x \in \Omega \rightarrow x(x) \in \mathbb{R}, w \in L^2(\Omega)\right\} \\ M &= \left\{m : x \in \Gamma \rightarrow m(x) \in \mathbb{R}, m \in L^2(\Gamma)\right\} \end{aligned} \tag{5}$$

The sets V, W and M are infinite dimensional. One can define finite-dimensional subsets for reconstructing u and q. Let us define V_h, W_h, M_h such that

$$\begin{aligned} &V_h \subset V, \quad \dim(V_h) = m_V \\ &W_h \subset W, \quad \dim(W_h) = m_W \\ &M_h \subset M, \quad \dim(M_h) = m_M \end{aligned} \tag{6}$$

A set of linearly independent vectors can be defined for each of these subspaces. They will be denoted in the following by $\tau_i \in V_h, i = 1, 2, ..., m_V$, $\varphi_i \in W_h, i = 1, 2, ..., m_W$ and $\mu_i \in M_h, i = 1, 2, ..., m_M$, and be called the basis functions of the space. An example of subspace V_h is the set of polynomial of degree $\leq m_V$, whose basis function can be composed of Lagrange polynomials of degree m_V. In this work, Dubiner's monomial basis is used.

D. Weak formulation

Equation 1 can be rewritten by considering the gradient of the variables as an unknown of the problem

$$\begin{aligned}
&\partial_t u(x,t) + \nabla \cdot F(u(x,t), q(x,t)) = S(u(x,t), q(x,t)), && x \in \Omega, && t \in \mathbb{R}_0^+ \\
&q(x,t) = \nabla u(x,t), && x \in \Omega, && t \in \mathbb{R}_0^+ \\
&u(x,t) = u_{bc}(x,t), && x \in \partial\Omega_d, && t \in \mathbb{R}_0^+ \\
&q(x,t) \cdot n = q_{n,bc}(x,t), && x \in \partial\Omega_n, && t \in \mathbb{R}_0^+ \\
&u(x,0) = U(x), && x \in \Omega
\end{aligned} \tag{7}$$

The weak formulation of Eq. (7) is written (if $(\tau, \varphi) \in V \times W$)

$$\begin{aligned}
&\sum_K \int_{\Omega_K} (\partial_t u^K - S^K)\varphi^K - F^K \nabla\varphi^K dV + \sum_K \int_{\partial\Omega_K \setminus \partial\Omega} F^K(u,q) \cdot n^K \varphi^K dS + \int_{\partial\Omega} F_n^K(u, u_{bc}, q, q_{n,bc}, n^K)\varphi^K dS = 0 \\
&\sum_K \int_{\Omega_K} q^K \tau^K + u^K \nabla\tau^K dV - \sum_K \int_{\partial\Omega_K \setminus \partial\Omega} u^K n^K \tau^K dS - \int_{\partial\Omega} u_{bc}^K n^K \tau^K dS = 0
\end{aligned} \tag{8}$$

where the spatial and temporal dependence of variables and vectors have been omitted in order to avoid clutter and the upper script K denotes the restriction of a function on the domain $\Omega_K \in \mathcal{T}$. We also have defined the normal component of the physical flux $F_n = F \cdot n$.

E. Weak formulation

Let us define the functions $\hat{u}_h^K$ and $\hat{q}_h^K$

$$\hat{u}_h^K = \begin{cases} \lambda_h^{K,K'} & \text{on } \partial\Omega_K \cap \partial\Omega_{K'} \\ u_{bc,h}^K & \text{on } \partial\Omega_K \cap \partial\Omega_d \\ u_h^K & \text{on } \partial\Omega_K \cap \partial\Omega \setminus \partial\Omega_d \end{cases} \tag{9}$$

and

$$\hat{q}_h^K = \begin{cases} q_h^K & \text{on } (\partial\Omega_K \cap \partial\Omega_{K'}) \cup (\partial\Omega_K \cap \partial\Omega \setminus \partial\Omega_n) \\ q_{n,bc,h}^K & \text{on } \partial\Omega_K \cap \partial\Omega_n \end{cases}. \tag{10}$$

where the λ variables are called the hybrid unknowns. As discussed below, the functions $\hat{u}_h$ and $\hat{q}_h$ will play an important role in the multi-physics version of HDG. They will be discussed later. In HDG, the discretized version of Eq. (8) is given by

$$\begin{aligned}
&\sum_K \int_{\Omega_K} (\partial_t u_h^K - S^K)\varphi_i^K - F^K \nabla\varphi_i^K dV + \sum_K \int_{\partial\Omega_K} \mathcal{H}(u_h^K, q_h^K, \hat{u}_h^K, \hat{q}_h^K, n^K)\varphi_i^K dS = 0 && i = 1, 2, ..., m_W \\
&\sum_K \int_{\Omega_K} q_h^K \tau_i^K + u_h^K \nabla\tau_i^K dV - \sum_K \int_{\partial\Omega_K} \hat{u}_h^K n^K \tau_i^K dS = 0 && i = 1, 2, ..., m_V \\
&\sum_{e \in \Gamma} \int_e \left[\mathcal{H}(u_h^{K_e}, q_h^{K_e}, \lambda_h^{K_e,K'_e}, q_h^{K_e}, n^{K_e}) + \mathcal{H}(u_h^{K'_e}, q_h^{K'_e}, \lambda_h^{K_e,K'_e}, q_h^{K'_e}, n^{K'_e}) \right] \mu_i^{K_e,K'_e} dS = 0 && i = 1, 2, ..., m - M
\end{aligned} \tag{11}$$

The superscript K, K' denotes the restriction of a function on the facet shared by Ω_K and $\Omega_{K'}$. The solution is reconstructed in a finite element-manner:

$$u_h = \sum_{i=1}^{m_W} u_i \varphi_i, \qquad q_h = \sum_{i=1}^{m_V} q_i \tau_i \qquad \lambda_h = \sum_{i=1}^{m_M} \lambda_i \mu_i. \tag{12}$$

Ω_{K_e} and $\Omega_{K'_e}$ represents the elements who share the facet e as a boundary. Finally, the physical flux at the element interfaces is discretized using a numerical flux function

$$F_n^K \simeq \mathcal{H}(u^K, q^K, \hat{u}_h^K, \hat{q}_h^K, n^K) \tag{13}$$

This formulation has many similar features as a classic DG formulation. First, it employs a high-order interpolation of the solution over the elements. Second, information is transmitted from one element to another through numerical fluxes. However, since the method contains an additional set of degrees of freedom compared to classic DG, it requires an additional set of equation. It is given in Eq. (11) by the conservation of the numerical flux through the traces

$$\sum_{e\in\Gamma}\int_e \left[\mathcal{H}(u_h^{K_e}, q_h^{K_e}, \lambda_h^{K_e,K'_e}, q_h^{K_e}, n^{K_e}) + \mathcal{H}(u_h^{K'_e}, q_h^{K'_e}, \lambda_h^{K_e,K'_e}, q_h^{K'_e}, n^{K'_e})\right] \mu_i^{K_e,K'_e} dS = 0 \quad i = 1, 2, ..., m_M \tag{14}$$

which ensures the conservativity of the method.

The addition of the hybrid degrees of freedom allows for the decomposition of the full problem into two tasks. The first one is to solve many small problems located at each element. The second one is to solve a globally coupled problem, which links all hybrid unknowns.

F. Solution strategy

The solution strategy of HDG, is described in this section. Eq. (11) can be solved using a Newton's method. It can be rewritten in the form

$$\mathcal{N}_h(x_h^n; y_i) = 0 \tag{15}$$

where $x^n = (\lambda_h^n, u_h^n, q_h^n)$ and $y_i = (\mu_i, \varphi_i, \tau_i)$. The purpose of Newton's iteration is to find a solution to the linearized problem

$$\mathcal{N}'_h(x_h^n; y_i)\delta x_h^n = -\mathcal{N}_h(x_h^n; y_i) \tag{16}$$

from an initial guess x_h^0. Once the solution x_h^n is obtained, the value of x_h^n is used as initial guess to solve for $x_h^{n+1} = x_h^n + \delta x_h^n$. Equation (16) can be conveniently written in matrix form

$$\underbrace{\begin{pmatrix} A & B & R \\ C & D & S \\ M & N & L \end{pmatrix}}_{\mathcal{N}'_h(x_h^n;y_i)} \overbrace{\begin{pmatrix} \delta Q \\ \delta U \\ \delta\Lambda \end{pmatrix}}^{\delta x_h^n} = \underbrace{\begin{pmatrix} F \\ G \\ H \end{pmatrix}}_{-\mathcal{N}_h(x_h^n;y_i)} = \begin{pmatrix} -\mathcal{R}_1 \\ -\mathcal{R}_2 \\ -\mathcal{R}_3 \end{pmatrix}, \tag{17}$$

where all the matrices of Eq. (17) are defined in Appendix A, and $\mathcal{R}_j,\ j = 1, 2, 3$ is the residual of an equation. Because each element exchanges information through the trace using the numerical flux, each element is only indirectly coupled to its neighbours via the trace variables. In other words, the submatrix

$$\Sigma = \begin{pmatrix} A & B \\ C & D \end{pmatrix} \tag{18}$$

is block diagonal. The size of each block does not exceed the number of degrees of freedom on the element. Equation (17) can be rewritten in two sets of equations:

$$\begin{pmatrix} A & B \\ C & D \end{pmatrix} \begin{pmatrix} \delta Q \\ \delta U \end{pmatrix} = \begin{pmatrix} \delta F \\ \delta G \end{pmatrix} - \begin{pmatrix} \delta R \\ \delta S \end{pmatrix} \delta\Lambda \tag{19}$$

and

$$\begin{pmatrix} L & M \end{pmatrix} \begin{pmatrix} \delta Q \\ \delta U \end{pmatrix} + N\delta\Lambda = H \tag{20}$$

By eliminating the local variables from Eq. (20) with the help of Eq. 19, one gets a system for the hybrid unknowns:

$$\left(N - \begin{pmatrix} L & M \end{pmatrix} \begin{pmatrix} A & B \\ C & D \end{pmatrix}^{-1} \begin{pmatrix} \delta R \\ \delta S \end{pmatrix}\right) \delta\Lambda = H - \begin{pmatrix} L & M \end{pmatrix} \begin{pmatrix} A & B \\ C & D \end{pmatrix}^{-1} \begin{pmatrix} \delta F \\ \delta G \end{pmatrix} \tag{21}$$

This system can be efficiently solved by constructing the local matrices and invert them on the spot while building the global matrix. Then, the global system Eq. (21) is solved and the hybrid unknowns are used to reconstruct the local ones. The solution algorithm to solve the full HDG system is given in Algorithm 1. Note that $\mathcal{R}$ represents the residual of the global system Eq. (21).

Algorithm 1 Solution procedure for HDG

Initialize λ_h, w_h, q_h;
while $||\mathcal{R}||_2 > \varepsilon$ **do**
  for i = 1,..., N_e **do**
    Assemble local system (Eq. (19));
    Solve local system;
    Store local solution;
    Assemble global system (Eq. (21));
  end for
  Solve global system;
  Update λ_h, w_h, q_h;
end while

IV. Hybridized discontinuous Galerkin method for multi-physics problems

This Section describes the extension of single-physics to multi-physics HDG. First, the basic assumptions of the method are described. Then, the spatial discretization and functional spaces are presented. Finally, the treatment of the interfaces between domain is discussed, along with the algorithm of the method.

A. Hypotheses on multi-physics problems

In this work, multi-physics problems are governed by different sets of equations that act on different but fixed spatial locations. Those domains exchange information through their common boundaries, called the interface boundary. The interface is fixed in time. In the following rationale, the mesh matches at the interface between two physical domains. The exploration of non-conforming meshes, moving or cell-cutting boundaries (like immersed boundary methods) for HDG are not treated here. Finally, only non-overlapping domains are considered.

To fix the idea, let us consider two non-overlapping domains Ω_1 and Ω_2 governed by different physics. For instance, in the conjugate heat transfer (CHT) model, Ω_1 would be a channel where a fluid flows and the Navier-Stokes equations apply, while Ω_2 would be the solid pipe surrounding the channel, where the heat diffusion equation governs the heat transfer phenomena. Both media have a common interface, which is called here $\Gamma_{1,2}$. The two physics are linked by interface conditions. In the case of CHT, the normal heat flux through the interface is conserved, while the temperature at the interface is continuous across the boundary between domains. On the other hand, a boundary condition has to be imposed on velocity and pressure, since in our model no information is transmitted from the velocity and pressure fields of the Navier-Stokes domain to the solid pipe. The crucial point of multi-domain simulations is the treatment of those information exchange and boundary condition imposition between two physical models. We will see that HDG is particularly well suited for these types of problems.

B. Continuous formulation

The multi-physics problem can be defined as a collection of single-physics problems. Let us consider a domain $\Omega^l \subset \mathbb{R}^D$ of dimension D with boundary $\partial\Omega^l$. Let us define the conservation equation over Ω^l:

$$\begin{aligned}
&\partial_t u^l(x,t) + \nabla \cdot F^l(u(x,t), \nabla u^l(x,t)) = S^l(u^l(x,t), \nabla u^l(x,t)), && x \in \Omega^l, && t \in \mathbb{R}_0^+ \\
&u^l(x,t) = u^l_{bc}(x,t), && x \in \partial\Omega^l_d, && t \in \mathbb{R}_0^+ \\
&\nabla u^l(x,t) \cdot n = q^l_{n,bc}(x,t), && x \in \partial\Omega^l_n, && t \in \mathbb{R}_0^+ \\
&u^l(x,0) = U^l(x), && x \in \Omega^l
\end{aligned} \tag{22}$$

Note that all symbols retain the same meaning as in Section III.A, but the superscript $l = 1, 2, ..., N_d$ denotes the subdomain under consideration.

C. Spatial discretization and functional spaces

Now, let us consider N_d distinct physical problems on N_d non-overlapping domains Ω^l. Consequently,

$$\Omega = \bigcup_{l=1}^{N_d} \Omega^l \tag{23}$$

The spatial discretization for each domain Ω^l is performed in the same way as for the single-physics case

$$\mathcal{T}^l = \bigcup_K \Omega_K^l, \quad \text{and} \quad \Omega_K^l \bigcap \Omega_{K'}^l = \emptyset \quad \text{if} \quad \Omega_K^l \neq \Omega_{K'}^l \quad l = 1, 2..., N_d \tag{24}$$

Similarly, the set of boundary elements $\partial\mathcal{T}^l$ is defined as

$$\partial\mathcal{T}^l = \{\partial\Omega_K \backslash \partial\Omega^l : \Omega_K \in \mathcal{T}^l\} \tag{25}$$

and the mesh skeleton Γ^l

$$\Gamma^l = \{e : e = \Omega_K^l \cap \Omega_{K'}^l \text{ for } \Omega_K^l, \Omega_{K'}^l \in \mathcal{T}^l, \Omega_K^l \neq \Omega_{K'}^l\} \tag{26}$$

In addition to the previously defined set of traces, we also define the set of traces on the interface between physical domains $\Gamma^{l,l'}$:

$$\Gamma^{l,l'} = \{e : e = \Omega_K \cap \Omega_{K'} \text{ for } \Omega_K \in \mathcal{T}^l, \Omega_{K'} \in \mathcal{T}^{l'}\}, \quad l, l' = 1, 2, ..., N_d \tag{27}$$

The same functional spaces as for the single-physics case are used here. See Section III.C for more details.

D. Weak formulation discretization

The weak formulation of the problem is obtained very similarly as for the single-physics case. Assuming $l = 1, 2, ..., N_d$, it is written in its most general form as

$$\begin{aligned}
&\sum_K \int_{\Omega_K^l} (\partial_t u_h^{l,K} - S^{l,K})\varphi_i^K - F^{l,K}\nabla\varphi_i^K dV + \sum_K \int_{\partial\Omega_K^l} \mathcal{H}^l(u_h^{l,K}, q_h^{l,K}, \hat{u}_h^{l,K}, \hat{q}_h^{l,K})\varphi_i^K dS = 0, \ i = 1, ..., m_W \\
&\sum_K \int_{\Omega_K^l} q_h^{l,K}\tau_i^K + u_h^{l,K}\nabla\tau_i^K dV - \sum_K \int_{\partial\Omega_K^l} \hat{u}_h^{l,K} n^K \tau_i^K dS = 0, \ i = 1, ..., m_V \\
&\sum_{e\in\Gamma^l\cup\Gamma^{l,l'}} \int_e \mathcal{F}^l(u_h^{l,K_e}, q_h^{l,K_e}, \lambda_h^{l,K_e,K'_e}, q_h^{l,K_e}, n^{K_e}; u_h^{l,K'_e}, q_h^{l,K'_e}\lambda_h^{l,K_e,K'_e}, q_h^{l,K'_e}, n^{K'_e})\mu_i^{K_e,K'_e} dS = 0, \ i = 1, ..., m_M
\end{aligned} \tag{28}$$

Once again, all symbols keep their previous definition, with the superscript l denoting the subdomain. Equation (28) has a very similar form as Eq. (11), but differ mainly in the transmission condition between elements, here represented by the function $\mathcal{F}^l$. On an internal facet in Γ^l (*i.e.* a facet that neither a frontier between two domain or a boundary), such function reduces to the conservation of the numerical flux through the trace, and one gets

$$\mathcal{F}^l = \mathcal{H}^l(u_h^{l,K_e}, q_h^{l,K_e}, \lambda_h^{l,K_e,K'_e}, q_h^{l,K_e}, n^{K_e}) + \mathcal{H}(u_h^{l,K'_e}, q_h^{l,K'_e}, \lambda_h^{l,K_e,K'_e}, q_h^{l,K'_e}, n^{K'_e}), \forall e \in \Gamma^l \tag{29}$$

On the other hand, on $\Gamma^{l,l'}$, the compatibility conditions can be more complex. Indeed, nothing guarantees that the number of degrees of freedom on the trace and on the element boundary correspond. Let's take once again the example of CHT. Let us consider two elements on both side of a domain interface. The number of unknowns on the fluid side is greater than the number of unknowns on the solid side, since the Navier Stokes equations solve for (p, u, T) while the heat equation only solves for T. Since only the heat flux is transmitted through the domain interface, the only required hybrid unknowns there are the ones associated with temperature. Consequently, the flux conservation will only apply to temperature, while classic boundary conditions will be applied on the remaining flow fields.

The previous examples treats with continuous fields across interfaces. This has for consequences to define a common set of hybrid unknowns for temperature at the facet interface of CHT problems. But this is not always the case. For instance, in electromagnetic field applications, the normal component of the electric field is not conserved, while the electric diffusive flux across the interface is. In those cases, the number of hybrid degrees of freedom on the domain interfaces needs to be doubled to take into account the jump in the electric field. Additional compatibility conditions have to be imposed on these degrees of freedom in order to guarantee the solvability of the system.

Consequently, the system can be rewritten in the form

$$
\begin{aligned}
&\sum_K \int_{\Omega_K^l} (\partial_t u_h^{l,K} - S^{l,K})\varphi_i^K - F^{l,K}\nabla\varphi_i^K \, dV + \sum_K \int_{\partial\Omega_K^l} \mathcal{H}^l(u_h^{l,K}, q_h^{l,K}, \hat{u}_h^{l,K}, \hat{q}_h^{l,K})\varphi_i^K \, dS = 0 \\
&\sum_K \int_{\Omega_K^l} q_h^{l,K}\tau_i^K + u_h^{l,K}\nabla\tau_i^K \, dV - \sum_K \int_{\partial\Omega_K^l} \hat{u}_h^{l,K} n^K \tau_i^K \, dS = 0 \\
&\sum_{e\in\Gamma^l\cap\Gamma^{l,l'}_{cont.}} \int_e \left[\mathcal{H}^l(u_h^{l,K_e}, q_h^{l,K_e}, \lambda_h^{K_e,K'_e}, q_h^{l,K_e}, n^{K_e}) + \mathcal{H}^l(u_h^{l,K'_e}, q_h^{l,K'_e}, \lambda_h^{K_e,K'_e}, q_h^{l,K'_e}, n^{K'_e})\right] \mu_i^{K_e,K'_e} dS \\
&+ \sum_{e\in\Gamma^{l,l'}_{disc}} \int_e \left[\mathcal{H}^l(u_h^{l,K_e}, q_h^{l,K_e}, \lambda_h^{l,K_e,K'_e}, q_h^{l,K_e}, n^{K_e}) + \mathcal{H}^{l'}(u_h^{l',K'_e}, q_h^{l',K'_e}, \lambda_h^{l',K_e,K'_e}, q_h^{l',K'_e}, n^{K'_e})\right] \mu_i^{K_e,K'_e} dS \\
&+ \sum_{e\in\Gamma^{l,l'}_{disc}} \int_e C^l(u_h^{l,K_e}, q_h^{l,K_e}, \lambda_h^{l,K_e,K'_e}, q_h^{l,K_e}, n^{K_e}; u_h^{l',K'_e}, q_h^{l',K'_e}\lambda_h^{l',K_e,K'_e}, q_h^{l',K'_e}, n^{K'_e})\mu_i^{K_e,K'_e} dS = 0
\end{aligned}
\tag{30}
$$

where we have defined $\Gamma^{l,l'}_{cont.}$ and $\Gamma^{l,l'}_{disc.}$ the portions of $\Gamma^{l,l'}$ where the transmitted variable are continuous and discontinuous across the interface respectively, and C the compatibility function that links the doubled hybrid unknowns from each side of the facet. To fix the idea, let us consider the particular case of two media whose interface surface charge is q_s. The normal component of the electric field has a discontinuity that can be described as

$$
E_1 n_1 + E_2 n_2 = \frac{q_s}{\varepsilon_0} \tag{31}
$$

where ε_0 is the void electric permittivity. In that particular case, the function C is defined as

$$
C = E_{\lambda^1} n_1 + E_{\lambda^2} n_2 - \frac{q_s}{\varepsilon_0} \tag{32}
$$

Since the problem has been now discretized, the next Section deals with the solution strategy.

E. Solution strategy

The previous Sections have given the main features of multi-physics HDG. The solution strategy of Eq. (30) is now discussed. In this work, a monolithic strategy has been chosen, meaning that the system is solved as a whole. In that way, the solution strategy for this multi-physics solver is exactly the same as the single-physics one. Indeed, Algorithm 1 is slightly modified in order to take into account the multiple models. The complete solution procedure is given in Algorithm 2.

Algorithm 2 Solution procedure for multi-domain HDG

```
Initialize λ_h, w_h, q_h;
while ||R||_2 > ε do
    for l = 1, ..., N_d do
        for i = 1,..., N_e do
            Assemble local system (Eq. (19)) of subdomain l;
            Solve local system of subdomain l;
            Store local solution of subdomain l;
            Assemble global system (Eq. (21));
        end for
    end for
    Solve global system;
    Update λ_h, w_h, q_h;
end while
```

Consequently, the multi-physics aspect of the problem modifies only the interface relation, but not the solution strategy nor the local solver, preserving all the features of the HDG method.

V. Applications

This section deals with the application of the solver to two test cases. The first one, the conjugate heat transfer problem, is a well-known multi-physics problem with analytical solution, and allows to study the continuous field transmission across the interfaces. Then, we apply the multi-physics solver to the complex case of inductively coupled plasma and compare our computations to the results of previous codes.

A. Conjugate heat transfer

The conjugate heat transfer problem is a well-known academic problem. A schematic is given in Fig. 1. A fluid flows in heat-conducting pipe. The upper wall of the pipe is at constant temperature T_{wall}. The lateral walls of the pipe are adiabatic. At the inlet of the channel, the analytical temperature and velocity profile are prescribed in order to match the analytical solution described below. The centre line of the pipe is axisymmetric while the exit is at a given constant pressure p_0. Finally, at the interface, the heat flux is conserved while a no-slip wall boundary condition is applied to the velocity field. The problem can be decoupled in three parts: the pipe, the solid and the interface domains.

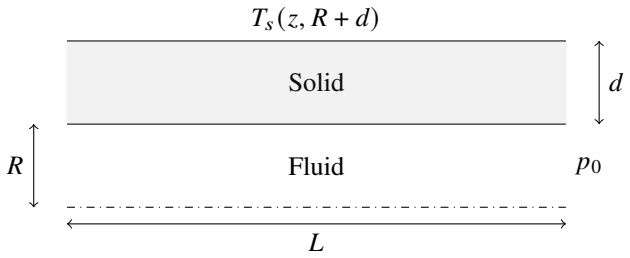

Fig. 1 Illustration of the conjugate heat transfer problem. The pipe is made of a solid material with finite thickness. Heat is exchanged between the solid and the fluid, resulting in equilibrium fully-developed steady-state temperature and velocity profiles.

Flow in the pipe The conjugate heat transfer problem is usually studied in the case of constant thermodynamic properties. This leads to a polynomial temperature profile of degree 4 and a polynomial velocity profile of degree 2 in the pipe, limiting the convergence study of such test case to polynomial interpolations of degree 3 and 1 respectively, since for higher order interpolation the solution is exactly captured by the solver. Instead, we found an analytical solution for the temperature and velocity profiles in the case where the viscosity η_f and thermal conductivity k_f of the fluid vary as

$$\begin{aligned} \eta_f(T) &= \eta_{f,0}\left(\frac{T_0}{T}\right)^2 \\ k_f(T) &= k_{f,0}\frac{T}{T_0} \end{aligned} \tag{33}$$

with $\eta_{f,0}$ and $k_{f,0}$ a constant viscosity and thermal conductivity respectively. In this particular case, if the density of the fluid is constant, the temperature and velocity profiles in the pipe can be expressed in terms of Bessel and generalized hypergeometric functions by solving the system

$$\begin{aligned} \partial_t(\rho_f u) + \nabla\cdot(\rho_f uu + p\mathbb{I} - \tau) &= 0 \\ \partial_t(\rho_f c_p T_f) + \nabla\cdot(\rho_f c_p T_f u + pu - \tau\cdot u) + \nabla\cdot(k_f \nabla T_f) &= 0 \end{aligned} \tag{34}$$

where ρ_f is the constant fluid density, p is the static pressure, u is the velocity vector, and $c_{p,f}$ is the heat capacity at constant pressure. Solving these equations for a steady state fully developed fluid leads to the following expressions for the temperature profile (see Appendix B for full developments and definition of the parameters showing in the following equations)

$$T_f = T_{interf}\left[\frac{J_0\left(\frac{r^2}{2\sqrt{\beta}}\right)}{J_0\left(\frac{R^2}{2\sqrt{\beta}}\right)}\right]^{\frac{1}{2}} \tag{35}$$

where J_0 is a Bessel function of the first kind and β is a constant parameter depending on thermodynamics, geometry of the problem and the constant pressure gradient. On the other hand, the velocity profile is given by

$$u(r) = \frac{\partial_z p}{4\eta_0}\left(\frac{T_{interf}}{T_0}\right)^2 \frac{\left[r^2\ {}_1F_2(\frac{1}{2};1,\frac{3}{2};-\frac{r^4}{16\beta}) - R^2\ {}_1F_2(\frac{1}{2};1,\frac{3}{2};-\frac{R^4}{16\beta})\right]}{J_0\left(\frac{R^2}{2\sqrt{\beta}}\right)} \tag{36}$$

where ${}_1F_2$ is a generalized hypergeometric function. As in the constant thermodynamic coefficient case, the pressure is linearly decreasing along the pipe of length L such that

$$\partial_z p = \partial_z p(\beta, k_{f,0}, \eta_{f,0}, T_0) \tag{37}$$

Solid side On the solid side, only an equation for temperature conduction is solved, namely

$$\rho_s C_s \partial_t T - \nabla \cdot (k_s \nabla T) = 0 \tag{38}$$

with C_s the heat capacity of the solid, ρ_s the solid density and k_s the solid thermal conductivity. The analytical solution of this problem at steady state is well known:

$$T_s = \left(T_{wall} - T_{interf}\right)\frac{\ln\left(\frac{r}{R}\right)}{\ln\left(1+\frac{d}{R}\right)} + T_{interf} \tag{39}$$

Interface The normal heat flux must remain constant at the fluid-solid interface

$$k_s \nabla T_s \cdot n = k_f \nabla T_f \cdot n \tag{40}$$

This condition allows to compute the value of the temperature at the interface between the solid and the fluid T_{interf}:

$$-\delta(d, R, \beta, k_f, k_s) T_{interf}^2 + T_{interf} - T_{wall} = 0 \tag{41}$$

where δ is a constant parameter of the problem. Since the interface consists only of a continuous temperature and a conservation equation, the only hybrid degrees of freedom along the interface are the one related to temperature. All other variable are determined through a boundary condition.

Convergence study The convergence study has been performed for two versions of the compatibility condition. The first one consists of having only one set of hybrid unknowns associated to the the temperature and impose conservativity of the numerical flux through the interface. The second one consists of doubling the unknowns related to temperature at the interface, and to enforce conservativity of the numerical flux and the continuity of temperature across the interface. It is possible to define completely a test case by fixing the pressure gradient and the interface temperature T_{interf}, $\mu_{f,0}$, $k_{f,0}$, k_s, T_0 and the geometry of the problem. In this case, we chose the following parameters:

- $\mu_{f,0} = 1\times10^{-4}$ Pa s
- $\partial_z p = -3.5\times10^{6}$ Pa
- $T_0 = 350\,\mathrm{K}$
- $T_{interf} = 0.1\delta^{-1}$
- $R = 1.5\times10^{-4}\mathrm{m}$
- $d = 2\times10^{-5}\mathrm{m}$
- $k_{f,0} = 0.01\,\mathrm{Wm^{-1}K^{-1}}$
- $k_s = 0.02\,\mathrm{Wm^{-1}K^{-1}}$

The convergence history is similar in both cases in all parts of the domain. Moreover, for a polynomial basis of dimension p, the order of convergence $p+1$ is retrieved. The results are displayed in Fig. 2 and 3. The error norm used for these computations is the following:

$$E_2(||v - v_{analytical}||^2) = \frac{\int_\Omega ||v - v_{analytical}||^2 dV}{\int_\Omega ||v_{analytical}||^2 dV}. \tag{42}$$

Note that a Lax-Friederichs convective numerical flux and a Local Discontinuous Galerkin (LDG) numerical fluxes were used in the computations. The only difference between the models besides the interface treatment is that the first case has less degrees of freedom than the second one, meaning that it is more interesting with continuous field to have only one set of hybrid variables for temperature across the interface. Finally, the mesh used for the convergence study has only one element in the width direction since the flow is supposed to be steady state, and is refined only in the radial direction. The number of elements N on the graph is inversely proportional to h, the element size in the radial direction.

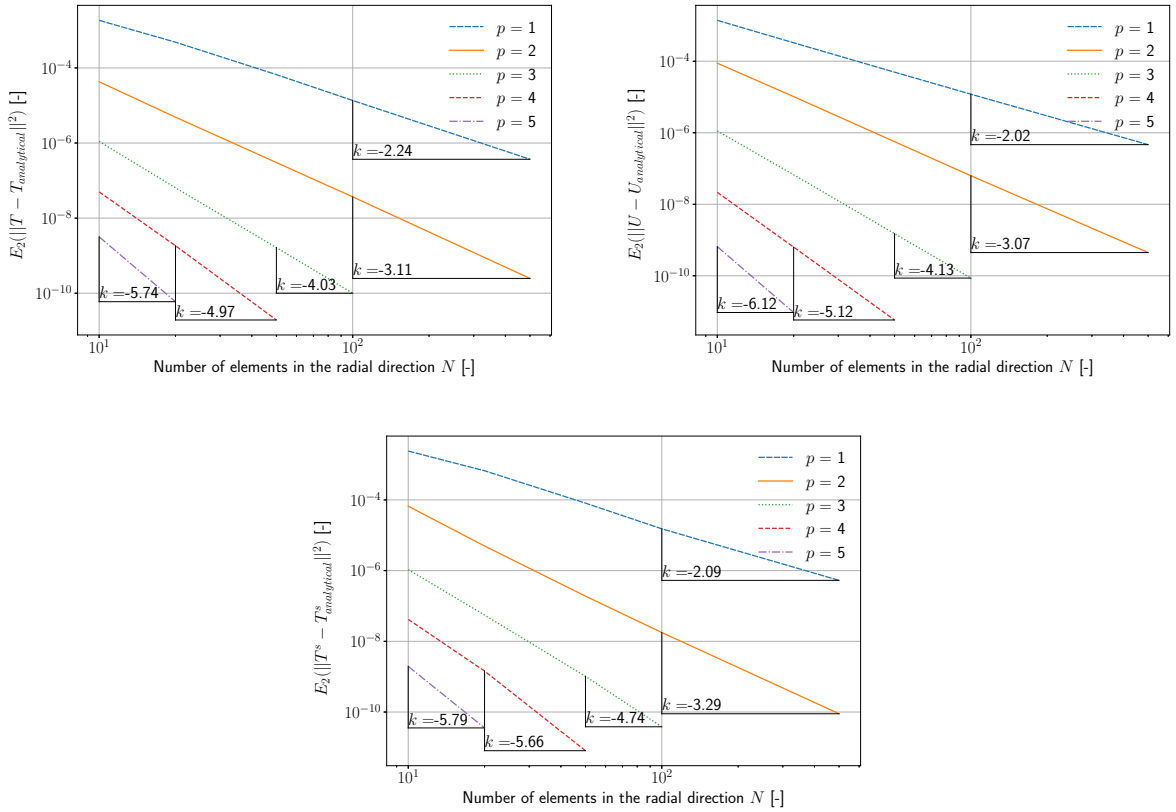

Fig. 2 Convergence study of the CHT problem. Each plot represents the convergence of the L_2 norm of the error of a scalar field as a function of the element number in the radial direction. On the top, from left to right, this error is represented for the temperature and velocity fields in the pipe. The bottom shows the error for the temperature field in the solid pipe. This convergence study has been performed for the case of single set of hybrid unknowns along the fluid-solid interface, requiring to impose only the conservativity of the numerical flux. p and k represent respectively the order of the polynomial interpolation of the solution of the approximation space and the order of convergence. The error norm $E_2(||v - v_{analytical}||^2)$ used is the ratio between $L_2(||v - v_{analytical}||^2)$ and $L_2(||v_{analytical}||^2$ and is thus dimensionless.

B. Inductively coupled plasma

We apply the method developed here to the case of inductively coupled plasma (ICP). A schematic representation of ICP is given in Fig. 4. ICP flows are very challenging to simulate as they require to capture large temperature gradients while dealing with non constant thermodynamic properties. Indeed, in the most powerful ICP facility in the world, it is possible to reach temperatures of 11 000 K inside the torch, while keeping the walls of the facility cooled down to 350 K.

The working principle of an ICP facility is the following: first, an electric arc ionises a gas (usually air, or argon). Then, an alternating current flowing through the coils surrounding the facility heats the fluid by Joule effect, creating a partially ionised plasma. These plasmas have numerous spatial application, such as the study of ablation on reentry material or the study of the demise of space debris. In this work, we are only interested in the torch part, where the heating takes place. The test section, or the chamber, where the jet expands and the probe is placed, will not be discussed here.

The equations solved in this section are derived from Navier-Stokes and Maxwell's equations accompanied by the classic assumptions made on ICP (see for instance [1] for a complete description of the assumptions), meaning that

- The flow is purely axisymmetric. All 3D effects are neglected. In particular, the coil is assumed to be composed of parallel current loops flowing through infinitely thin wires. The impact of the coil configuration was shown to

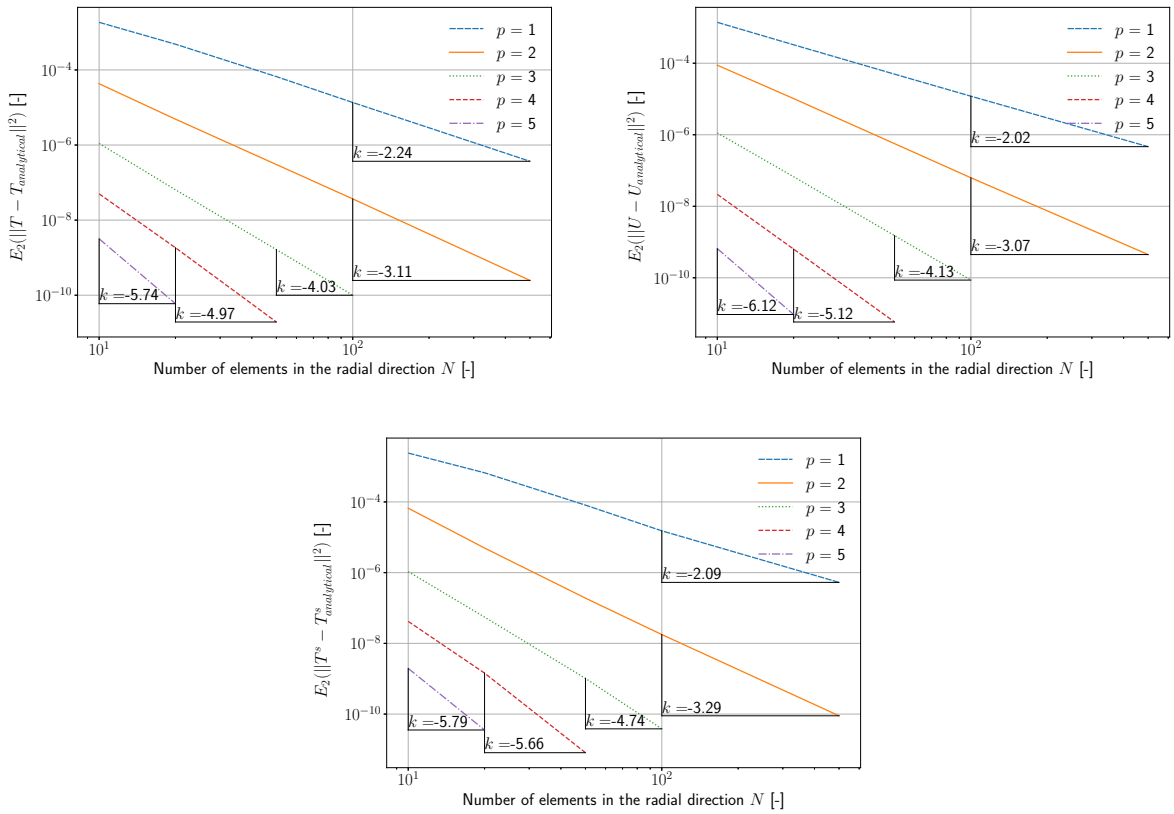

Fig. 3 Convergence study of the CHT problem. Each plot represents the convergence of the L_2 norm of the error of a scalar field as a function of the element number in the radial direction. On the top, from left to right, this error is represented for the temperature and velocity fields in the pipe. The bottom shows the error for the temperature field in the solid pipe. This convergence study has been performed for the case of doubled hybrid unknowns along the fluid-solid interface, requiring to impose the continuity of the temperature in addition to the conservativity of the numerical flux. p and k represent respectively the order of the polynomial interpolation of the solution and the order of convergence. The error norm $E_2(||v - v_{analytical}||^2)$ used is the ratio between $L_2(||v - v_{analytical}||^2)$ and $L_2(||v_{analytical}||^2$ and is thus dimensionless.

have an impact on the torch symmetry[9]. These effects will be ignored here.

- The electric field is purely azimuthal. This results from the assumption that there is no diffusion current in the axisymmetric plane (ambipolar assumption).
- The problem is at local thermodynamic equilibrium (LTE), meaning that the chemical reaction time is much smaller than the characteristic flow time. Comparisons between experimental studies and finite volumes code computations showed that this assumption holds in the range of pressure studied here to some extent [10], but the hypothesis must be relaxed when the pressure in the facility decreases [11].
- All flow quantities are averaged over one oscillation frequency of the excitation current. Solving with the complete time oscillation of the induction current means that the electromagnetic wave propagation must be captured. Since they travel at the speed of light, the numerical problem becomes very stiff, increasing the computational costs. Moreover, decreasing the time step of the simulation would require to capture non-equilibrium chemistry, as the simulation time would become much smaller than the reaction time. This lead has never been investigated before with an ICP code, and is not pursued here.
- We consider the problem at steady-state, neglecting all hydrodynamic and electromagnetic instabilities. Of course, it is well known that a hot plasma jet released in cold air gives rise to instabilities driven by static pressure of the facility and the ripple part of the induction current (see for instance [12–14]).

- We consider that the Lorentz force is negligible. The Lorentz force is the cause of instabilities for low-frequency and low pressure regimes. This is not the case for the application studied here [15].

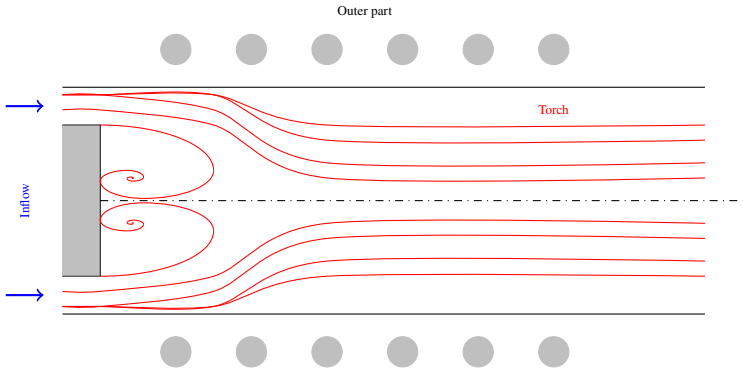

Fig. 4 Schematic representation of an inductively coupled plasma (ICP). The torch is surrounded by coils (the grey disks outside the torch) where an induction current flows. Inside the torch, a sample of streamlines has been represented. The injection system is annular in order to produce a recirculation close to the inlet, stabilizing the flow. It is also possible add a swirl component to the flow to further stabilize the torch.

ICP can be seen as a multi-domain problem. Indeed, one way of imposing a boundary condition on the electric field is to extend the computational domain beyond the torch, and to cancel the electric field sufficiently far away from the latter. This cuts the whole domain into two parts as shown in Fig. 5: the torch, where Maxwell and Navier-Stokes equations are solved, and the outer region, where only Maxwell equations are solved. As for CHT, we describe here the problem in three parts, the torch, the outer region and the interface. We then describe the various boundary conditions, the numerical flux used for the computations and the iterative procedure employed for computing the induction current.

Torch In the torch, the system of equation resulting from the previous assumptions is given by

$$\partial_t(rw) + \partial_z\left(rF_c^z(w) - rF_d^z(w,\nabla w)\right) + \partial_r\left(rF_c^r(w) - rF_d^r(w,\nabla w)\right) = rS(w,\nabla w) \tag{43}$$

where the state vector is

$$w = \begin{pmatrix} \rho & \rho u_z & \rho u_r & \rho u_\theta & \rho e + \rho\frac{u^2}{2} & E_P \end{pmatrix}^T, \tag{44}$$

the convective flux vector is given by

$$\begin{aligned} F_c^z &= \begin{pmatrix} \rho u_z & \rho u_z^2 + p & \rho u_z u_\theta & \rho e u_z + \frac{u^2}{2}u_z + p u_z & 0 \end{pmatrix}^T \\ F_c^r &= \begin{pmatrix} \rho u_r & \rho u_z u_r & \rho u_\theta u_r \rho e u_r + \frac{u^2}{2}u_r + p u_r & 0 \end{pmatrix}^T \end{aligned} \tag{45}$$

,

the diffusive flux vector is given by

$$\begin{aligned} F_d^z &= \begin{pmatrix} 0 & \tau_{zz} & \tau_{zr} & \tau_{z\theta} & \tau_{zz}u_z + \tau_{zr}u_r + \tau_{z\theta}u_\theta - q_z & \partial_z\left(rE_P\right) \end{pmatrix}^T \\ F_d^r &= \begin{pmatrix} 0 & \tau_{rz} & \tau_{rr} & \tau_{r\theta} & \tau_{rz}u_z + \tau_{rr}u_r + \tau_{r\theta}u_\theta - q_r & \partial_r\left(rE_P\right) \end{pmatrix}^T, \end{aligned} \tag{46}$$

and the source terms are given by

$$S = \begin{pmatrix} 0 & 0 & \frac{p+\rho u_\theta^2 - \tau_{\theta\theta}}{r} & \frac{-\rho u_r u_\theta}{r} & P_J & E_p + \frac{2i\pi f \mu_0 \sigma_e (E_c + E_P)}{r} \end{pmatrix}^T. \tag{47}$$

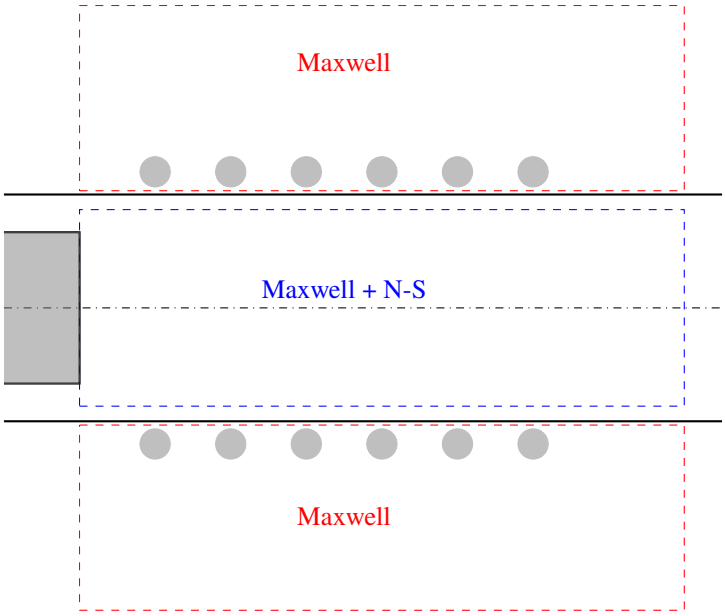

Fig. 5 Domain decomposition of inductively coupled plasmas in the HDG code. In the torch, Maxwell and Navier-Stokes equations are solved. The domain is extended beyond the torch so the electric field is cancelled sufficiently far away from the torch. In this extension region, called the outer region, only Maxwell's equations are solved.

with σ_e the electric conductivity of the plasma, μ_0 the magnetic permeability of the void and f the oscillation frequency of the induction current. The viscous stress tensor is then given by

$$\begin{aligned}
\tau_{zz} &= 2\eta\left(\partial_z u_z - \frac{1}{3}\nabla\cdot u\right)\\
\tau_{rz} &= \tau_{zr} = \eta\left(\partial_z u_r + \partial_r u_z\right)\\
\tau_{z\theta} &= \eta\partial_z u_\theta\\
\tau_{rr} &= 2\eta\left(\partial_r u_r - \frac{1}{3}\nabla\cdot u\right)\\
\tau_{r\theta} &= \eta\left(\partial_r u_\theta - \frac{u_\theta}{r}\right)\\
\tau_{\theta\theta} &= 2\eta\left(\frac{u_r}{r} - \frac{1}{3}\nabla\cdot u\right)
\end{aligned}, \tag{48}$$

The velocity divergence in cylindrical coordinates is given by

$$\nabla\cdot u = \partial_z u_z + \frac{1}{r}\partial_r(r u_r) \tag{49}$$

and the power dissipated by Joule effect is

$$P_J = \frac{\sigma_e}{2}\left(Re(E_I)^2 + Im(E_I)^2\right) \tag{50}$$

where

$$E_I = E_C + E_P \tag{51}$$

with E_C the electric field produced by a coil and E_P the electric field produced in reaction in the plasma. Analytical solutions exist for E_C, see for instance [16]. The interested reader can refer to [1] for a complete derivation of the equations governing the ICP flows.

Concerning the thermodynamics of the torch, the library Mutation++ [17] is used. The library uses table of coefficients delivered by NASA in order to compute the thermo-physical properties of matter. Since the system is considered to be at local thermodynamic equilibrium, the mixture's equilibrium has to be found, which is computationally expensive. In order to address this issue, a table of equilibrium states is pre-computed, and the values are linearly interpolated in this table, accelerating the computations.

Outer region In the outer region, only the electric field is computed. Since the air is almost a perfect electric insulator at ambient temperature, the following equation is solved:

$$\partial_z(r\partial_z E_P) + \partial_r(r\partial_r E_P) = \frac{E_P}{r}. \tag{52}$$

Interface The electric field being tangential to the interface, it is continuous. Since it is the only transmitted quantity between the fluid and solid domains, only the hybrid degrees of freedom associated with the electric field are solved there. The continuity of the normal numerical flux has to be imposed for the electric field, while boundary conditions on the velocity, pressure and temperature fields have to be imposed.

Boundary conditions The boundary conditions are the following:

Maxwell far field

$$E_P = 0 \tag{53}$$

Axis of symmetry

$$\partial_r p = 0, \quad \partial_r u_z = 0, \quad u_r = 0, \quad \partial_r T = 0 \quad E_P = 0 \tag{54}$$

Outlet

$$p = p_0, \quad \partial_z u_z = 0, \quad \partial_z u_r = 0, \quad \partial_z T = 0 \tag{55}$$

Inlet wall

$$u = 0, \quad T = T_{wall} \tag{56}$$

Inlet

$$u = U_{in}(r) \tag{57}$$

with $U_{in}(r)$ the radial velocity inlet profile.

Interface wall The electric field numerical flux is conserved across the interface and

$$u = 0, \quad T = T_{wall}. \tag{58}$$

Note that all quantities that are not imposed are copied from the inside.

Numerical flux In the simulation of ICP, the choice of the numerical flux is of paramount importance, since the problem is very subsonic ($M \simeq 10^{-4}$). At such low-mach number, the density of the mixture is mostly determined by the temperature of the fluid, making the residual of the continuity equation almost pressure-independent. To overcome this issue and better condition the system, a family of low Mach AUSM numerical convective flux has been developed [1, 18, 19]. Such numerical flux can be written as follows

$$\mathcal{H}^c(w, \lambda, n) = \frac{1}{2}\left(m_{1/2} + m_p\right)(\Psi_w + \Psi_\lambda) - \frac{1}{2}|m_{1/2}|\,(\Psi_\lambda - \Psi_w) + P_{1/2} \tag{59}$$

where Ψ is a vector of convected quantities

$$\Psi = \begin{pmatrix} 1 & u_\perp & u_\parallel & u_\theta & e + \frac{1}{2}u^2 + \frac{p}{\rho} \end{pmatrix}^T \tag{60}$$

with $u_\perp$ and $u_\parallel$ the perpendicular and parallel velocity to the facet under consideration. One defines

$$m_{1/2} = \frac{1}{4}(\rho_w + \rho_\lambda)(\Psi_\lambda + \Psi_w) \tag{61}$$

and

$$P_{1/2} = \begin{pmatrix} 0 & \frac{1}{2}(p_\lambda + p_w) & 0 & 0 & 0 \end{pmatrix}. \tag{62}$$

Finally, m_p is a pressure diffusion term stabilizing the flow

$$m_p = -\frac{p_\lambda - p_w}{V_p} \tag{63}$$

where V_p is a preconditionning velocity, chosen here as $V_p = U_{max}$, with U_{max} the greatest value of the inflow velocity. A classic local discontinuous Galerkin solver is used for the diffusive part of the flux.

Iterative procedure for computing the induction current and initial conditions In ICP flows, only the power dissipated in the facility by Joule effect is known. Since there is no analytical relation linking the induction current to the power dissipated in the facility, one must determine the excitation current through an iterative procedure. For steady-state solution, the procedure employed is the following one:

1) Solve the problem for one Newton iteration.
2) Compute the total power dissipated in the torch.
3) If the computed power does not match the target power, the induction current I_c is updated. Knowning that the power dissipated in the facility is such that

$$P_J \propto I_c^2, \tag{64}$$

a new induction current is computed such that

$$I_c^{k+1} = I_C^k \sqrt{\frac{P_J^{target}}{P_J}} \tag{65}$$

The procedure is stopped once P_J is sufficiently close to P_J^{target}. Concerning the initialization of the field, the induction current is first set to 1 A, while a constant longitudinal velocity is applied everywhere in the torch. A parabolic temperature profile is imposed, rising from the wall temperature to the highest expected temperature in the torch.

Comparison with previous ICP code The code developed here has been compared to results computed by Vanden Abeele with a finite volumes code [20]. The test case consists of an ICP torch of Argon. The geometry of the torch is given in Fig. 6.

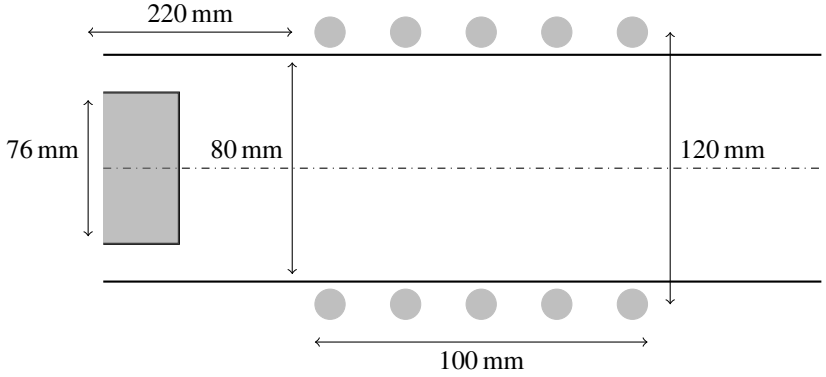

Fig. 6 Geometry of the argon ICP torch. The schematic is not at scale.

Argon is injected at a pressure of 0.1 atm and a flow rate of 2.8 g s^{-1} with a swirl of $S = 45°$. Note that the swirl velocity u_θ verifies the relation $\frac{u_z}{u_\theta} = S$, where S is expressed in radians. The power to be dissipated in the facility is $P_J^{target} = 10$ kW, and the oscillation frequency is $f = 27$ MHz. The comparison between the HDG ICP code with a polynomial interpolation of degree 4 and the previous finite volumes code is given in Fig. 7. Small discrepancies are observed close to the inlet. This is not surprising, as the finite volumes code uses an adiabatic wall at the inlet while we used an isothermal wall boundary condition.

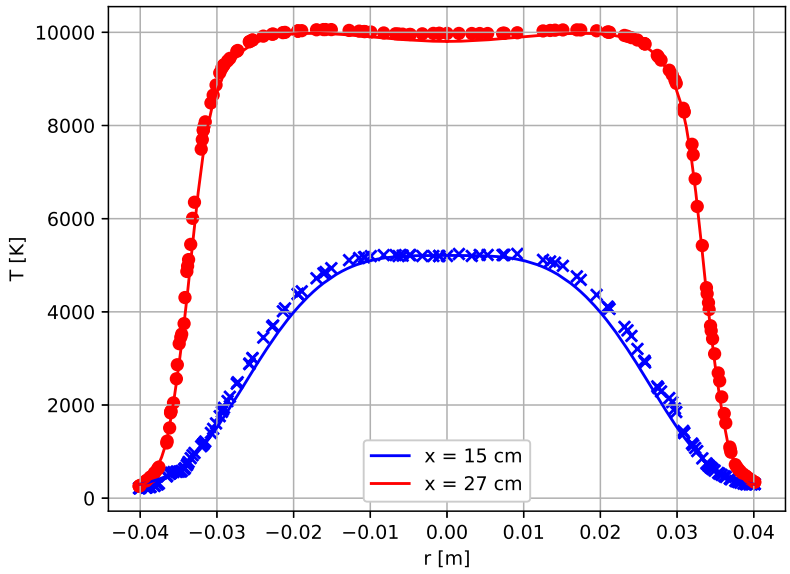

Fig. 7 Comparison between the finite volumes (crosses and dots) and HDG (continuous lines) ICP codes radial (r) temperature profiles for two axial positions (x) (close to the inlet (15 cm) and mid-torch (27 cm)). The solution has been computed with a polynomial interpolation of degree 2.

Although the code has been verified on an ICP test case, some problems related to the ICP simulation with HDG still remain to be solved. In particular, two main issues arose during the simulations.

The first one is related to the conditioning of the matrix of the hybrid system which degrades as the mesh is refined. This problem is not only related to the ICP test case, but also on simple problems such as Poiseuille flows and CHT. This ill-conditioning leads to large iteration of the GMRES solver and slows down the computations drastically. The fix currently applied for this problem is to increase the filling of the ILU preconditioner, but this can only be a temporary solution as filling also increases the solution time. Moreover it was observed that they do not depend on the mesh refinement in the near-wall region.

On the other hand, oscillations of the temperature field were observed near the interface wall, especially close to the inlet and the regions of large temperature gradients. An example of such oscillations is given in Fig. 8. The origin of those wiggles has yet to be determined. These oscillations introduce spurious heat flux measurements at the wall.

On the otehr hand, an advantage of the HDG code compared to its finite volumes predecessor is that the mesh constraints can be relaxed (see Fig. 9 for a comparison between a finite volumes and a HDG mesh). While finite volumes solver required structured cells of a micrometre in the near-wall region in order to converge to a solution, HDG only requires cells of a millimetre in the same area.

VI. Conclusion

In this work, we presented a multi-domain version of a hybridized discontinuous Galerkin solver. We showed that the method developed keeps the solution strategy of a classic HDG single domain method.

We presented convergence tests on a conjugate heat transfer problem, and showed that we retrieved the expected convergence rates for two versions of the multi-domain. The first one consisted of defining only one set of hybrid unknowns at the interface boundary associated with the temperature, and to impose the conservativity of the normal component of the numerical flux across the interface. The second one doubled these degrees of freedom and imposed the continuity of temperature in addition to the flux conservativity. Both approaches gave similar results in terms of convergence.

Then, a more complex test case, involving inductively coupled plasma, was presented. These computations showed that the current HDG method is able to reproduce results from previous finite volumes codes. Moreover, it showed that

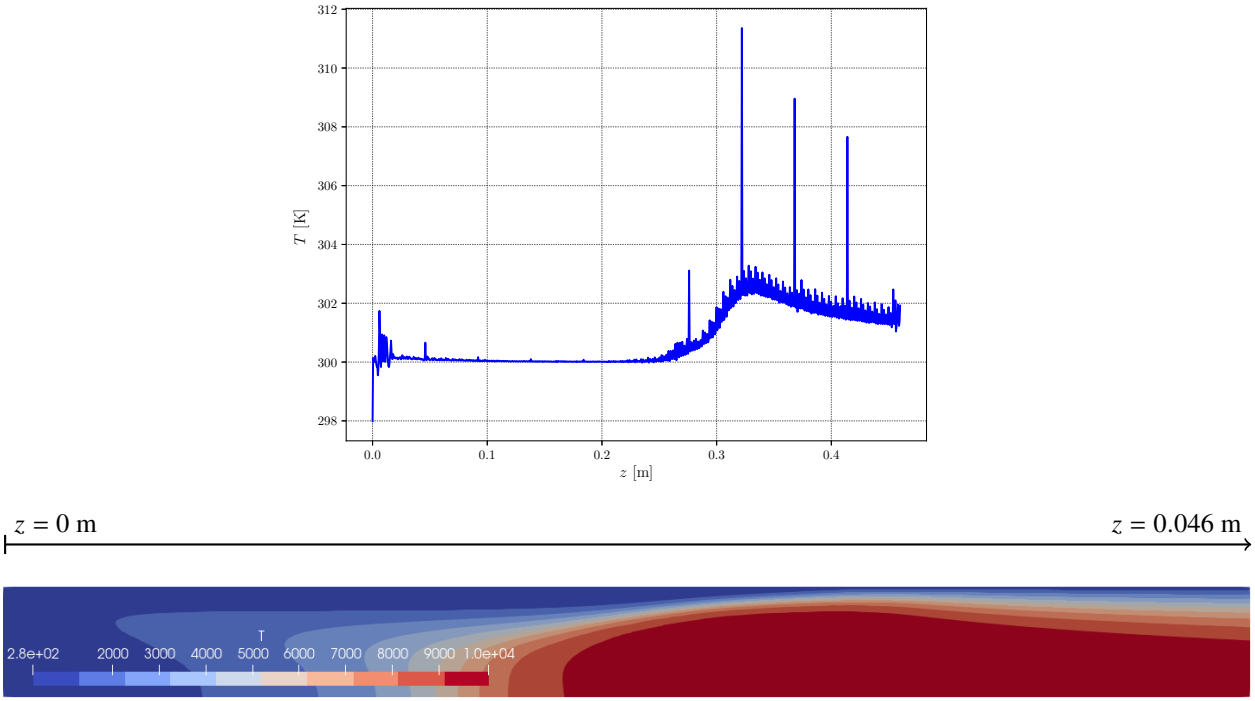

Fig. 8 Temperature profile in the z direction at the interface wall. Spurious oscillations occur close to the entry region ($z = 0$ m) and close to the highest temperature gradient region ($z = 0.32$ m). The nature of these oscillation is still under investigation. The contour plot represents the temperature distribution in the argon ICP torch.

the grid could be coarser in the near-wall region and the mesh could be triangular and unstructured, as opposed to the finite volumes case.

We also showed that the current implementation has spurious oscillations at the level of the interface boundary condition for the ICP test case. The conditioning of the problem degrades also with the mesh refinment. These are the two main problems to be addressed before continuing the ICP developments, as the former leads to spurious heat flux measurements at the wall, and the latter impinges the computational time.

Besides these main drawbacks, many topics have not been addressed in this paper. First, the multi-domain solver is only restricted to meshes with matching connections. The solver could be generalized to non-matching meshes, allowing to handle them separately. The code used here has *hp* adaptive algorithm implemented for single models. Extending the code to non-matching meshes would allow the use of these algorithms, automatizing the mesh generation. Another point is the code parallelisation, which has yet to be performed.

Another important topic is the study of unsteady phenomena, such as the hydrodynamic instabilities. The hot jet released in the cold chamber is the siege of Kelvin-Helmholtz instabilities that must be correctly captured. These instabilities can be influenced by the Lorentz force, which was completely disregarded here, or the static back pressure. Studying the impact of this force on the flow can be of a interest.

Final subjects of interest would be the comparison of the results this code produces with experimental data and a further assessment of the impact of the LTE assumption on the flow. However, these comparisons can be done only once the spurious wiggles have been corrected.

The list of points to be investigated given here is far from exhaustive. The study of non-equilibrium chemistry in ICP flows, the influence of the complete variation of flow quantities with the electric current or elemental de-mixing in local thermodynamic equilibrium are other examples of subjects to be explored. By developing this pioneering high-order solver, we hope to ease the study of these numerous topics.

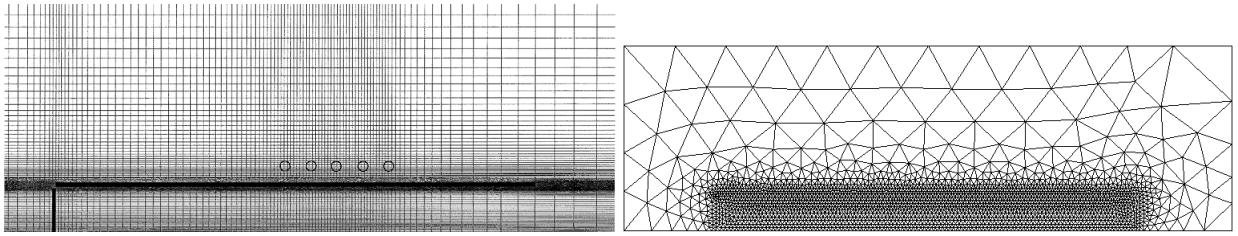

Fig. 9 Comparison between the finite volumes mesh (left) and the HDG mesh (right). While finite volumes requires very small elements at the upper wall (size of $1\ \mu m$) in order to converge, the HDG method is not so stringent as millimetre sized cells in the near wall region is sufficient.

A. Jacobian of the HDG system

The HDG method is linearized in the form of

$$\begin{pmatrix} A & B & R \\ C & D & S \\ L & M & N \end{pmatrix} \begin{pmatrix} \delta Q \\ \delta W \\ \delta \Lambda \end{pmatrix} = \begin{pmatrix} F \\ G \\ H \end{pmatrix} = \begin{pmatrix} -R_1 \\ -R_2 \\ -R_3 \end{pmatrix}. \tag{66}$$

with

$$\begin{aligned}
A = \frac{\partial R_1}{\partial q_l^K} &= \int_{\Omega_K} \tau_l \tau_i dV \\
B = \frac{\partial R_1}{\partial u_l^K} &= -\int_{\partial\Omega_K \cap \partial\Omega} \frac{\partial \hat{u}_j}{\partial u_l} \phi_l \tau_i \cdot n dS + \int_{\Omega_K} \phi_l \nabla \tau_i dV \\
R = \frac{\partial R_1}{\partial \lambda_l^L} &= -\int_L \mu_l [[\tau_l]] dS \\
C = \frac{\partial R_2}{\partial q_l^K} &= -\int_{\Omega_K} \frac{\partial S}{\partial q} \phi_i \tau_l + \frac{\partial F}{\partial q} \tau_l \nabla \phi_i dV + \int_{\partial\Omega_K} \frac{\partial \mathcal{H}}{\partial q} \tau_l \phi_i dS \\
D = \frac{\partial R_2}{\partial u_l^K} &= \int_{\Omega_K} \frac{\delta_{jl}}{\Delta t^K} - \frac{\partial S}{\partial u} \phi_l \phi_i - \frac{\partial F}{\partial u} \phi_l \nabla \phi_i dV + \int_{\partial\Omega_K} \frac{\partial \mathcal{H}}{\partial u} \phi_l \phi_i dS \\
S = \frac{\partial R_2}{\partial \lambda_l^L} &= \int_L \frac{\partial [[\mathcal{H}]]}{\partial \lambda} \mu_l \phi_i dS \\
L = \frac{\partial R_3}{\partial q_l^{K'}} &= \int_{\partial\Omega_K \cap \Gamma^0} \frac{\partial \mathcal{F}}{\partial q} \tau_l \mu_i^{\partial\Omega_K \cap \Gamma^0} dS \\
M = \frac{\partial R_3}{\partial u_l^K} &= \int_{\partial\Omega_K \cap \Gamma^0} \frac{\partial \mathcal{F}}{\partial u} \phi_l \mu_i^{\partial\Omega_K \cap \Gamma^0} dS \\
N = \frac{\partial R_3}{\partial \lambda_l^L} &= \int_L \frac{\partial [[\mathcal{F}]]}{\partial \lambda} \mu_l \mu_i dS
\end{aligned} \tag{67}$$

and R_1, R_2 and R_3 the residual of each equation and all other symbols keep their definition from Section IV.

B. Analytical solution of CHT problem with varying viscosity and thermal conductivity

We show here how an analytical solution to the axisymmetric incompressible conjugate heat transfer in a pipe of radius R surrounded by a pipe of thickness d can be found for particular expressions of the thermodynamic properties of the fluid. In particular, the viscosity η and heat conductivity k evolve according the power laws

$$\begin{aligned} \eta(T) &= \eta_0 \left(\frac{T}{T_0}\right)^n \\ k(T) &= k_0 \left(\frac{T}{T_0}\right)^m \end{aligned} \tag{68}$$

where n and m are real coefficients. The equations for the temperature T and the velocity u for incompressible flows have to be solved altogether:

$$\begin{aligned} &\frac{1}{r}\partial_r(r\eta\partial_r u) = \partial_z p \\ &\frac{1}{r}\partial_r\left(rk\partial_r T + r\eta u\partial_r u\right) = u\partial_z p \end{aligned} \tag{69}$$

where $\partial_z p$ is the constant temperature gradient along the pipe. Integrating the first equation yields

$$r\eta\partial_r u = \frac{\partial_z p}{2} r^2 + C_1 \tag{70}$$

Because $\partial_r u(0)$ is finite, $C_1 = 0$. Multiplying the momentum equation by u and injecting in the temperature equation yields

$$\frac{1}{r}\partial_r\left(rk\partial_r T + r\eta u\partial_r u\right) = \frac{u}{r}\partial_r(r\eta\partial_r u) \tag{71}$$

which, after simplification, yields

$$\partial_r\left(rk\partial_r T\right) + r\eta\left(\partial_r u\right)^2 = 0 \tag{72}$$

By injecting the integrated momentum equation in this result, one gets

$$\partial_r\left(rk\partial_r T\right) + \frac{r^3(\partial_z p)^2}{4\eta} = 0 \tag{73}$$

When injecting the expression for the viscosity and heat conductivity, we get

$$\frac{k_0}{T_0^m(m+1)}\partial_r\left(r\partial_r T^{m+1}\right) + \frac{r^3(\partial_z p)^2}{4\eta_0}\frac{T_0^n}{T^n} = 0 \tag{74}$$

Let us define α and β such that

$$\alpha = T^{m+1}, \qquad \beta = \frac{4\eta_0 k_0}{T_0^{m+n}(m+1)(\partial_z p)^2} \tag{75}$$

The equation becomes

$$\partial_r\left(r\partial_r\alpha\right) + \frac{r^3}{\beta}\alpha^{\frac{-n}{m+1}} = 0 \tag{76}$$

In the particular case of $\frac{-n}{m+1} = 1$,

$$\partial_r\left(r\partial_r\alpha\right) + \frac{r^3}{\beta}\alpha = 0 \tag{77}$$

and its general solution is a linear combination of Bessel functions of the first and second kind

$$T^{m+1} = C_1 J_0\left(\frac{r^2}{2\sqrt{\beta}}\right) + C_2 Y_0\left(\frac{r^2}{2\sqrt{\beta}}\right), \tag{78}$$

where

$$\begin{aligned} J_\alpha(x) &= \sum_{p=0}^{\infty} \frac{(-1)^p}{p!\Gamma(p+\alpha+1)}\left(\frac{x}{2}\right)^{2p+\alpha} \\ Y_\alpha(x) &= \frac{J_\alpha(x)\cos(\alpha\pi) - J_{-\alpha}(x)}{\sin(\alpha\pi)} \end{aligned} \tag{79}$$

with

$$\Gamma(z) = \int_0^\infty t^{z-1} e^{-t} dt \ , \quad z \in \mathbb{C}. \tag{80}$$

Note that, for z integer, one simply has

$$\Gamma(z) = (n-1)! \ , \quad z \in \mathbb{N}. \tag{81}$$

Since T is finite at the centerline, $C_2 = 0$ ($\lim_{x\to 0} Y_0(x) = -\infty$). On the other hand, at the fluid-solid interface, the temperature is the one at the interface so that

$$T_{interf}^{m+1} = C_1 J_0\left(\frac{R^2}{2\sqrt{\beta}}\right) \tag{82}$$

Consequenlty,

$$T^{m+1} = T_{interf}^{m+1} \frac{J_0\left(\frac{r^2}{2\sqrt{\beta}}\right)}{J_0\left(\frac{R^2}{2\sqrt{\beta}}\right)} \tag{83}$$

On the other hand, the velocity can be expressed as

$$\begin{aligned} \partial_r u &= \frac{\partial_z p}{2\eta_0} \frac{T_0^n}{T_{interf}^n} \left[\frac{J_0\left(\frac{R^2}{2\sqrt{\beta}}\right)}{J_0\left(\frac{r^2}{2\sqrt{\beta}}\right)}\right]^{\frac{n}{m+1}} r \\ &= \frac{\partial_z p}{2\eta_0} \frac{T_0^n}{T_{interf}^n} \frac{J_0\left(\frac{r^2}{2\sqrt{\beta}}\right)}{J_0\left(\frac{R^2}{2\sqrt{\beta}}\right)} r \end{aligned} \tag{84}$$

since it is assumed that $\frac{n}{m+1} = -1$. Now, integrating the equation and using the boundary condition $u(R) = 0$ yields

$$u(r) = \frac{\partial_z p}{4\eta_0} \frac{T_0^n}{T_{interf}^n} \frac{\left[r^2 \ {}_1F_2(\frac{1}{2}; 1, \frac{3}{2}; -\frac{r^4}{16\beta}) - R^2 \ {}_1F_2(\frac{1}{2}; 1, \frac{3}{2}; -\frac{R^4}{16\beta})\right]}{J_0\left(\frac{R^2}{2\sqrt{\beta}}\right)} \tag{85}$$

where

$${}_pF_q(a_1, ..., a_p; b_1, ..., b_q; z) = \sum_{n=0}^{\infty} \frac{\Pi_{i=0}^p \frac{\Gamma(a_i+n)}{\Gamma(a_i)}}{\Pi_{i=0}^q \frac{\Gamma(b_i+n)}{\Gamma(b_i)}} \frac{z^n}{n!} \tag{86}$$

is the generalized hypergeometric. Note that the maximal velocity and pressure gradient are linked by the relation

$$u(0) = u_{max} = -\frac{\partial_z p}{4\eta_0} \frac{T_0^n}{T_{interf}^n} \frac{R_1^2 F_2(\frac{1}{2}; 1, \frac{3}{2}; -\frac{R^4}{16\beta})}{J_0\left(\frac{R^2}{2\sqrt{\beta}}\right)} \tag{87}$$

Let us now find an expression for the interface temperature by using the continuity of the normal heat flux through the interface. The heat flux there seen from the fluid side is

$$\begin{aligned} k_f \partial_r T &= k_0 \frac{T_f^m}{T_0^m} \partial_r T_f \\ &= \frac{k_0}{(m+1) T_0^m} \partial_r T_f^{m+1} \\ &= \frac{-R k_0 T_{interf}^{m+1}}{\sqrt{\beta}(m+1) T_0^m} \frac{J_1\left(\frac{R^2}{2\sqrt{\beta}}\right)}{J_0\left(\frac{R^2}{2\sqrt{\beta}}\right)} \end{aligned} \tag{88}$$

The heat flux in the solid is a classic logarithmic profile:

$$T = (T_{wall} - T_{inter.})\frac{\ln\left(\frac{r}{R}\right)}{\ln\left(\frac{R+d}{R}\right)} + T_{inter.} \tag{89}$$

Equating this result with the heat flux in the solid yields

$$\frac{-Rk_0T_{interf}^{m+1}}{\sqrt{\beta}(m+1)T_0^m}\frac{J_1\left(\frac{R^2}{2\sqrt{\beta}}\right)}{J_0\left(\frac{R^2}{2\sqrt{\beta}}\right)} = k_s\frac{T_{wall} - T_{inter.}}{R\ln\left(\frac{R+d}{R}\right)} \tag{90}$$

Let us define

$$\delta = \frac{R^2k_0\ln(1+d/R)J_1\left(\frac{R^2}{2\sqrt{\beta}}\right)}{\sqrt{\beta}(m+1)T_0^mk_sJ_0\left(\frac{R^2}{2\sqrt{\beta}}\right)} \tag{91}$$

The equation for the interface temperature reduces to

$$-\delta T_{interf}^{m+1} + T_{interf} - T_{wall} = 0 \tag{92}$$

It can be interesting to specify the admissible values of T_{interf} in order to obtain a positive wall temperature, which is equivalent to have

$$T_{interf}(1 - \delta T_{interf}^m) > 0 \tag{93}$$

To simplify the computations, we consider the case $m = 1$. Since by the definition of Bessel functions and the variables of the problem, $\delta > 0$,

$$T_{interf} \in]0; \gamma^{-1}[\tag{94}$$

Outside of this interval, the wall temperature is supposed to be negative, which is unphysical. On the other hand, the temperature profile is supposed to be positive everywhere in the flow. Knowing that $r \in [0; R^2]$, it means that $\frac{R^2}{2\sqrt{\beta}}$ is at most the first zero of $J_0(x)$. Consequently, considering that $\beta > 0$

$$\beta > \frac{R^4}{4j_{0,1}^2} \tag{95}$$

where $j_{0,1}$ is the first zero of $J_0(x)$. This sharp limit leads to the following inequatlity for the pressure ($m = 1$)

$$(\partial_z p)^2 < \frac{8\eta_0k_0T_0j_{0,1}^2}{R^4} \tag{96}$$

Acknowledgments

The first author is supported by a fellowship from the Fund for Research Training in Industry and Agriculture (FRIA). This paper is born from the collaboration between the Université de Liège and the von Karman Institute for Fluid Dynamics.

References

[1] Magin, T., "A Model for Inductive Plasma Wind Tunnels," Ph.D. thesis, von Karman Institute for Fluid Dynamics, 2004.

[2] Lani, A., Villedieu, N., Bensassi, K., Kapa, L., Vymazal, M., Yalim, M. S., and Panesi, M., "COOLFluiD: An open computational platform for multi-physics simulation and research," *21st AIAA Computational Fluid Dynamics Conference*, 2013.

[3] Nguyen, N. C., Peraire, J., and Cockburn, B., "An implicit high-order hybridizable discontinuous Galerkin method for linear convection-diffusion equations," *Journal of Computational Physics*, Vol. 228, No. 9, 2009, pp. 3232–3254.

[4] Nguyen, N., Peraire, J., and Cockburn, B., "Hybridizable Discontinuous Galerkin Methods," *Spectral and High Order Methods for Partial Differential Equations*, edited by J. Hestaven and R. E.M., Springer, 2011, lecture no ed., pp. 63–84. https://doi.org/10.1007/978-3-642-15337-2.

[5] Giles, M. B., "Stability analysis of numerical interface conditions in fluid-structure thermal analysis," *International Journal for Numerical Methods in Fluids*, Vol. 25, No. 4, 1997, pp. 421–436.

[6] Verstraete, T., and Scholl, S., "Stability analysis of partitioned methods for predicting conjugate heat transfer," *International Journal of Heat and Mass Transfer*, Vol. 101, 2016, pp. 852–869.

[7] Hao, Z., Ren, X., Song, Y., and Gu, C., "An investigation of conjugate heat transfer simulations based on discontinuous Galerkin methods on unstructured grids," *Proceedings of the ASME Turbo Expo*, Vol. 3, No. August 2017, 2013. https://doi.org/10.1115/GT2013-94498.

[8] Woopen, M., May, G., and Schütz, J., "Adjoint-based error estimation and mesh adaptation for hybridized discontinuous Galerkin methods," *International Journal for Numerical Methods in Fluids*, Vol. 76, No. September, 2014, pp. 811–834.

[9] Bernardi, D., Colombo, V., Ghedini, E., and Mentrelli, A., "Three-dimensional modeling of inductively coupled plasma torches," *Pure and Applied Chemistry*, Vol. 77, No. 2, 2005, pp. 359–372. https://doi.org/10.1351/pac200577020359.

[10] Fagnani, A., Le Quang Huy, D., Helber, B., Demange, S., Turchi, A., Chazot, O., and Hubin, A., "Investigation of a free-stream air plasma flow by optical emission spectroscopy and comparison to magnetohydrodynamics simulations," *AIAA Scitech 2020 Forum*, Vol. 1 PartF, No. January, 2020, pp. 1–15. https://doi.org/10.2514/6.2020-0382.

[11] Zhang, W., Lani, A., and Panesi, M., "Analysis of non-equilibrium phenomena in inductively coupled plasma generators," *Physics of Plasmas*, Vol. 23, No. 7, 2016. https://doi.org/10.1063/1.4958326, URL http://dx.doi.org/10.1063/1.4958326.

[12] Cipullo, A., Helber, B., Panerai, F., and Chazot, O., "Experimental Characterization of the Free-stream Plasma Flow Produced bythe VKI Plasmatron Facility using Optical Emission Diagnostics," *RTO-EN-AVT-199, Paper 17, von Karman Institute, Rhode-Saint-Genèse, Belgium*, 2012, pp. 1–16.

[13] Cipullo, A., Helbert, B., Panerai, F., Zeni, L., and Chazot, O., "Investigation of Freestream Plasma Flow Produced by Inductively Coupled Plasma Wind Tunnel," *Journal of Thermophysics and Heat Transfer*, Vol. 28, No. 3, 2016, pp. 381–393. https://doi.org/10.2514/1.t5109.

[14] Demange, S., "Absolute instabilities in heated jets," Ph.D. thesis, Université Libre de Bruxelles, 2021. URL https://www.vki.ac.be.

[15] Smolyakov, A. I., Godyak, V. A., and Tyshetskiy, Y. O., "Nonlinear effects in inductively coupled plasmas," *Physics of Plasmas*, Vol. 10, No. 5 II, 2003, pp. 2108–2116. https://doi.org/10.1063/1.1566443.

[16] Jang, T., Seo, Y. K., Sohn, S. H., and Jung, J. W., "Calculation of the off-axes magnetic field for finite-length solenoids," *New Physics: Sae Mulli*, Vol. 70, No. 8, 2020, pp. 667–674. https://doi.org/10.3938/NPSM.70.667.

[17] Scoggins, J. B., Leroy, V., Bellas-Chatzigeorgis, G., Dias, B., and Magin, T. E., "Mutation++: MUlticomponent Thermodynamic And Transport properties for IONized gases in C++," *SoftwareX*, Vol. 12, 2020. https://doi.org/10.1016/j.softx.2020.100575.

[18] Liou, M. S., "A sequel to AUSM, Part II: AUSM+-up for all speeds," *Journal of Computational Physics*, Vol. 214, No. 1, 2006, pp. 137–170. https://doi.org/10.1016/j.jcp.2005.09.020.

[19] Vanden Abeele, D., and Degrez, G., "Efficient computational model for inductive plasma flows," *AIAA journal*, Vol. 38, No. 2, 2000, pp. 234–242. https://doi.org/10.2514/3.14402.

[20] Vanden Abeele, D., Vasil'evskii, S. A., Kolesnikov, A., Degrez, G., and Bottin, B., "Code-To-Code Validation of Inductive Plasma Computations," Tech. rep., von Karman Institute for Fluid Dynamics, St. Genesius-Rode, Belgium, 1999. https://doi.org/10.1615/itppc-1998.370.